Electronic Supplementary Material (ESI) for CrystEngComm.

Electronic Supporting Information

for

The Role of S-bond in Tenoxicam Keto-Enolic Tautomerization†

Sergey G. Arkhipov[a,b,c], Peter S. Sherin*[a,d], Alexey S. Kiryutin[a,d], Vladimir A. Lazarenko[e] and Christian Tantardini*[f]

---

[a] *Novosibirsk State University, Pirogova str. 2, 630090 Novosibirsk (Russian Federation).*
[b] *Boreskov Institute of Catalysis SB RAS Prospekt Akademika Lavrentyeva, 5, 630090 Novosibirsk (Russian Federation).*
[c] *Institute of Solid State Chemistry and Mechanochemistry SB RAS Kutateladze str. 18, 630128 Novosibirsk (Russian Federation).*
[d] *International Tomography Center Institutskaya 3a, 630090 Novosibirsk (Russian Federation).*
[e] *National Research Center "Kurchatov Institute" Akademika Kurchatova square 1, 123182, Moscow (Russian Federation).*
[f] *Center for Energy Science and Technology, Skoltech Skolkovo Institute of Science and Technology, Nobelya str. 3, 143026 Moscow (Russian Federation).*
*Corresponding to sherin@tomo.nsc.ru (Peter S. Sherin) and christiantantardini@ymail.com (Christian Tantardini).

† Dedicated to the memory of Dr. Alexey P. Chupakhin (1952-2018)

S1. Table of positions of maxima of absorption and fluorescence emission bands in wavelengths (λ_{max}^{abs}, λ_{max}^{flr}) and wavenumbers (v_{max}^{abs}, v_{max}^{flr}), Stokes shifts (Δv) and fluorescence quantum yields (Φ_F) of TXM in various solvents; dielectric constant of used solvents (ε) [1]. [a]

Solvent	ε	λ_{max}^{abs}/nm	λ_{max}^{flr}/nm	v_{max}^{abs} $/10^3 cm^{-1}$	v_{max}^{flr} $/10^3 cm^{-1}$	$\Delta v/10^3 cm^{-1}$	$\Phi_F/10^{-3}$
Cyclohexane	2.02	342	494	29.2	20.2	9.0	2.3
Dioxane	2.21	343	512	29.2	19.5	9.6	2.8
Toluene	2.38	346	500	28.9	20.0	8.9	2.2
Chloroform	4.89	345	492	29.0	20.3	8.7	2.1
THF	7.58	344	503	29.1	19.9	9.2	–*
Acetone	20.6	346	515	28.9	19.4	9.5	1.2
ACN	35.9	354	515	28.3	19.4	8.8	0.9
DMSO	46.4	386	540	25.9	18.5	7.4	–*

* not determined due to large contribution from impurity

[a] The Φ_F values were determinted with respect to kynurenine in aqueous solution, Φ_F (KN) = 8.2×10^{-3} [2].

S2. Picture of Absorption and fluorescence emission and excitation spectra recorded with TXM in cyclohexane, dioxane, toluene and acetone at different excitation and emission wavelengths.

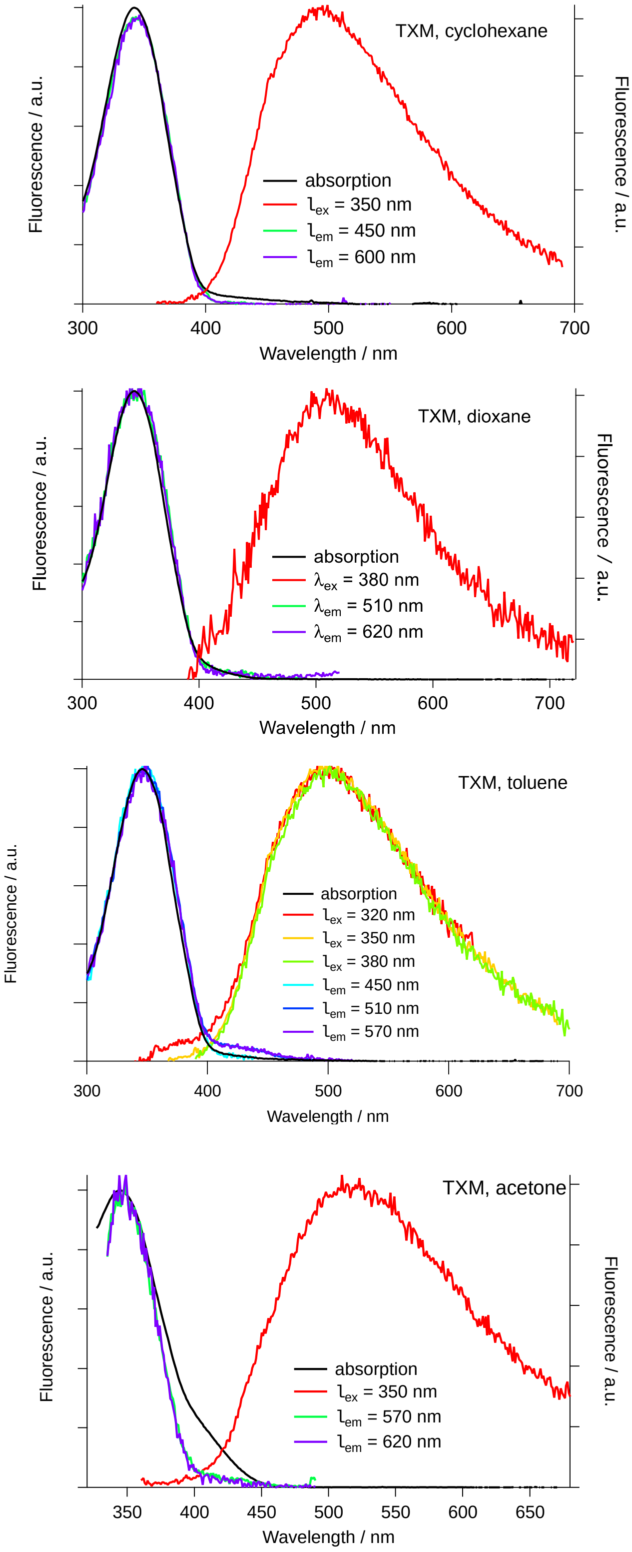

S3. Picture of fluorescence time profiles recorded with TXM in low polar solvents at 500 nm after the excitation at 375 nm.

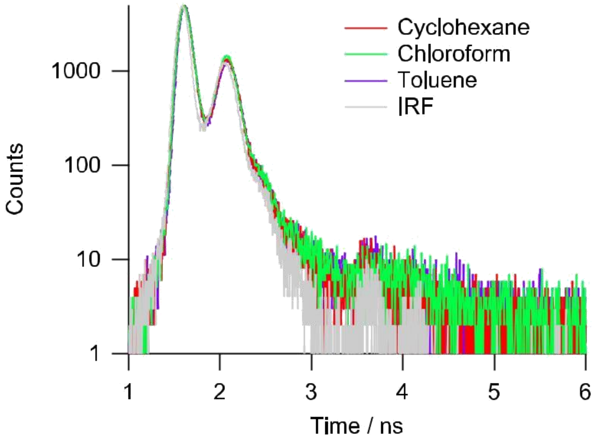

S4 Temperature influence on TXM absorption spectra in Acetonitrile and Chloroform.

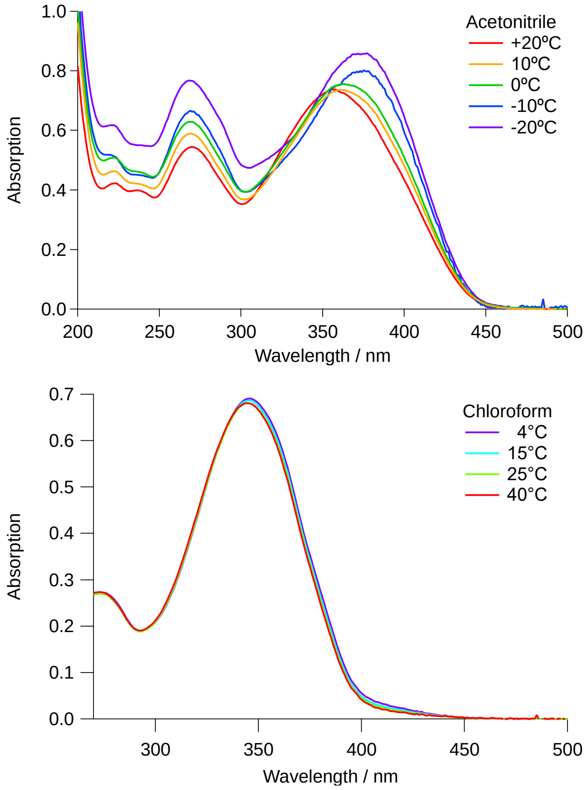

S5. Figure 700 MHz ^{1}H NMR spectrum of TXM in $CDCl_3$ at 25 °C. BKE form of TXM is predominant at high temperature. Assignments of all protons are shown on the spectrum.

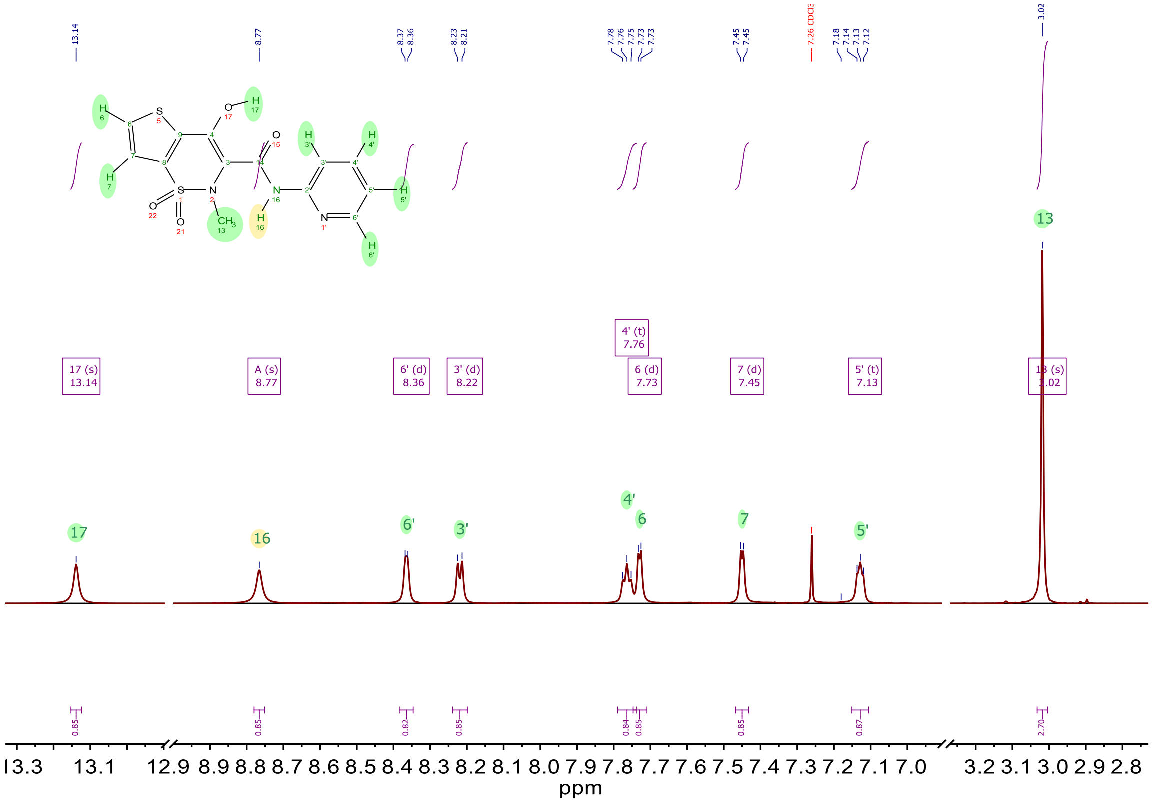

S6. Figure 176.1 MHz ^{13}C{1H} NMR spectrum of TXM in CDCl$_3$ at 25 °C. BKE form of TXM is predominant at high temperature. Assignments of all carbons are shown on the spectrum. To suppress all ^{13}C-^{1}H scalar couplings a broadband decoupling on proton channel was applied during acquisition.

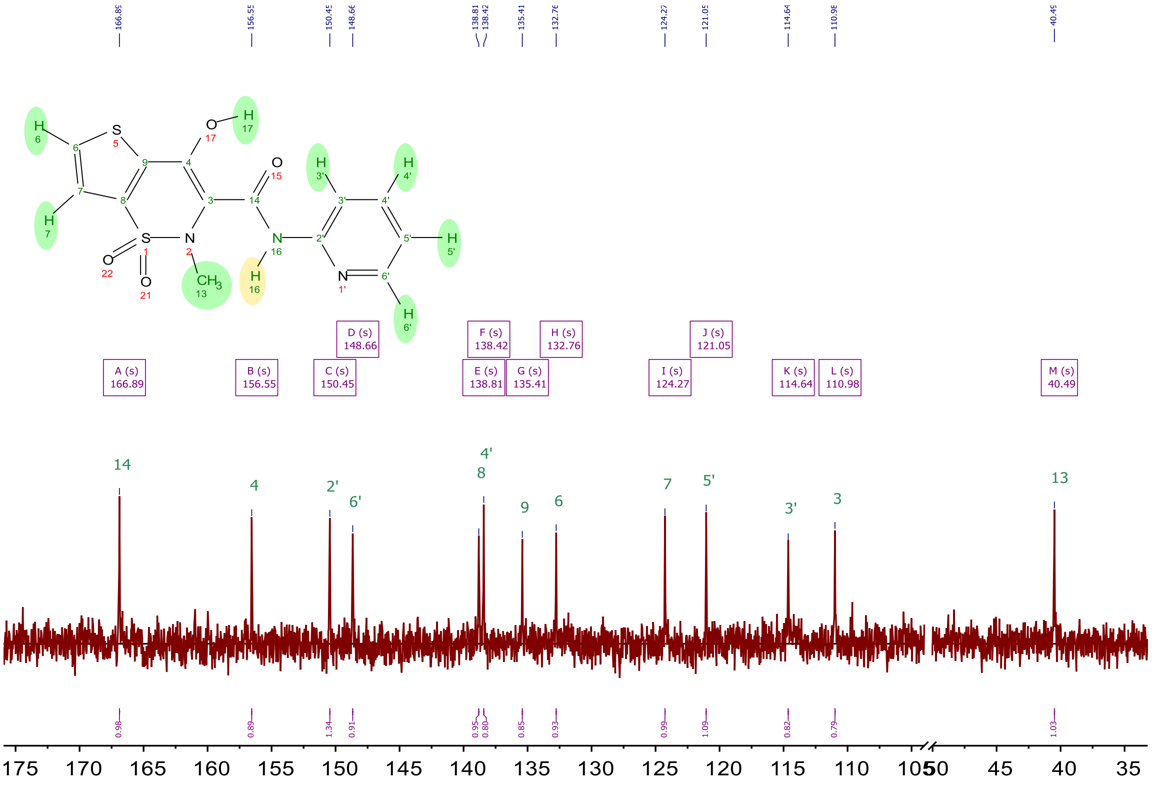

S7. Figure ^{1}H-^{13}C HSQC NMR spectrum of TXM in $CDCl_3$ at 25 °C. BKE form of TXM is predominant at high temperature. Cross-peaks in HSQC spectrum indicate correlation between directly bonded protons and carbons (C-H bonds).

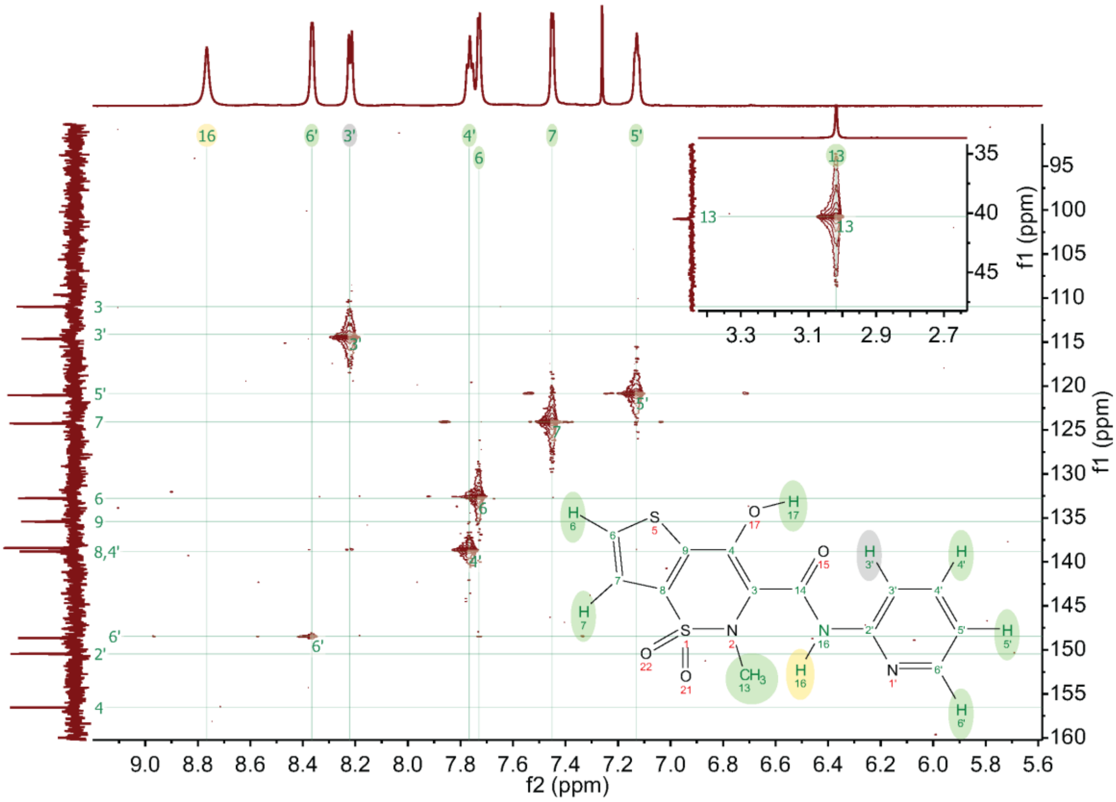

S8. Figure ^{1}H-^{13}C HMBC NMR spectrum of TXM in $CDCl_3$ at 25 °C. BKE form of TXM is predominant at high temperature. Cross-peaks in HMBC spectrum indicate correlation between protons and carbons separated by 2-4 covalent bonds, while direct correlation of single-bonded protons and carbons are suppressed. HMBC allows to assign quaternary carbons and carbonyl fragments.

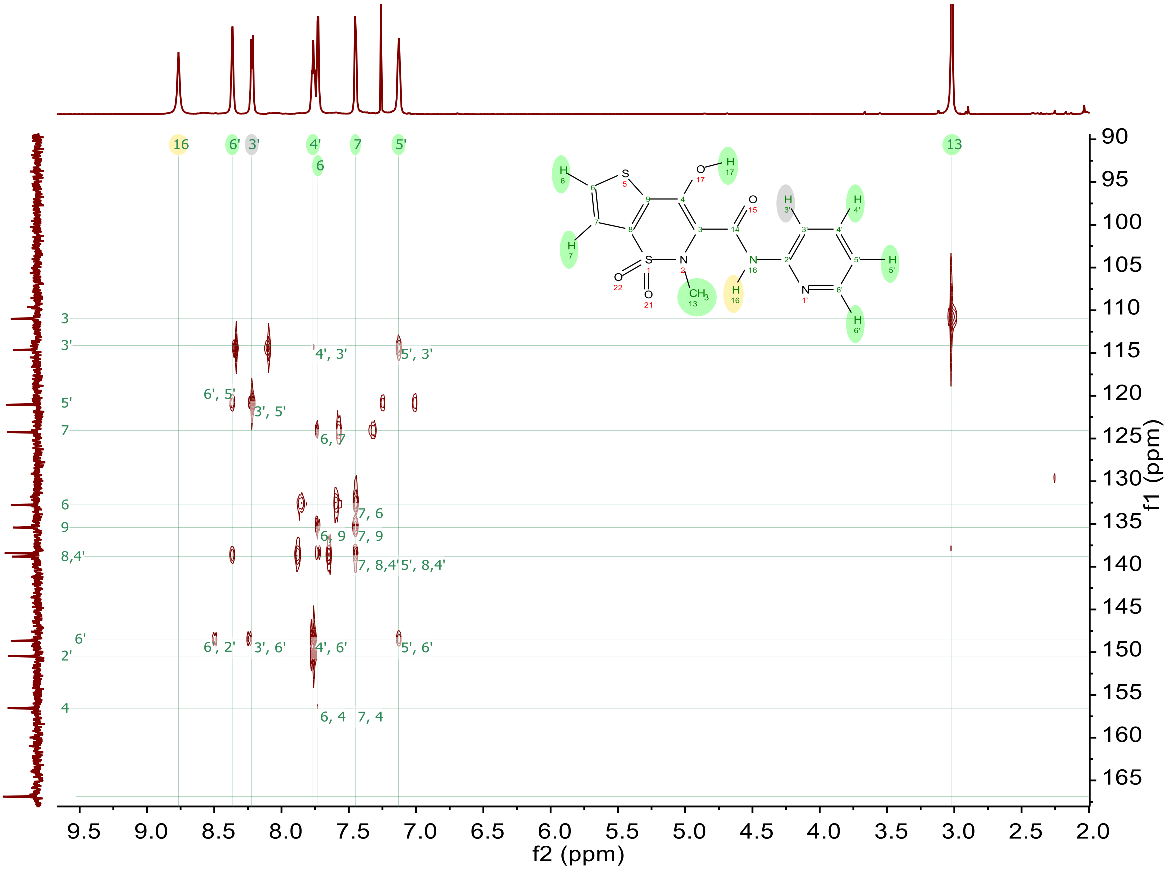

S9. Figure ^{1}H-^{15}N HSQC NMR spectrum of TXM in $CDCl_3$ at 25 °C. BKE form of TXM is predominant at high temperature. Cross-peaks in ^{1}H-^{15}N HSQC spectrum indicate correlation between directly bonded protons and nitrogens (N-H bonds). In BKE form we see only one cross-peaks assigned to H_{16} and N_{16}.

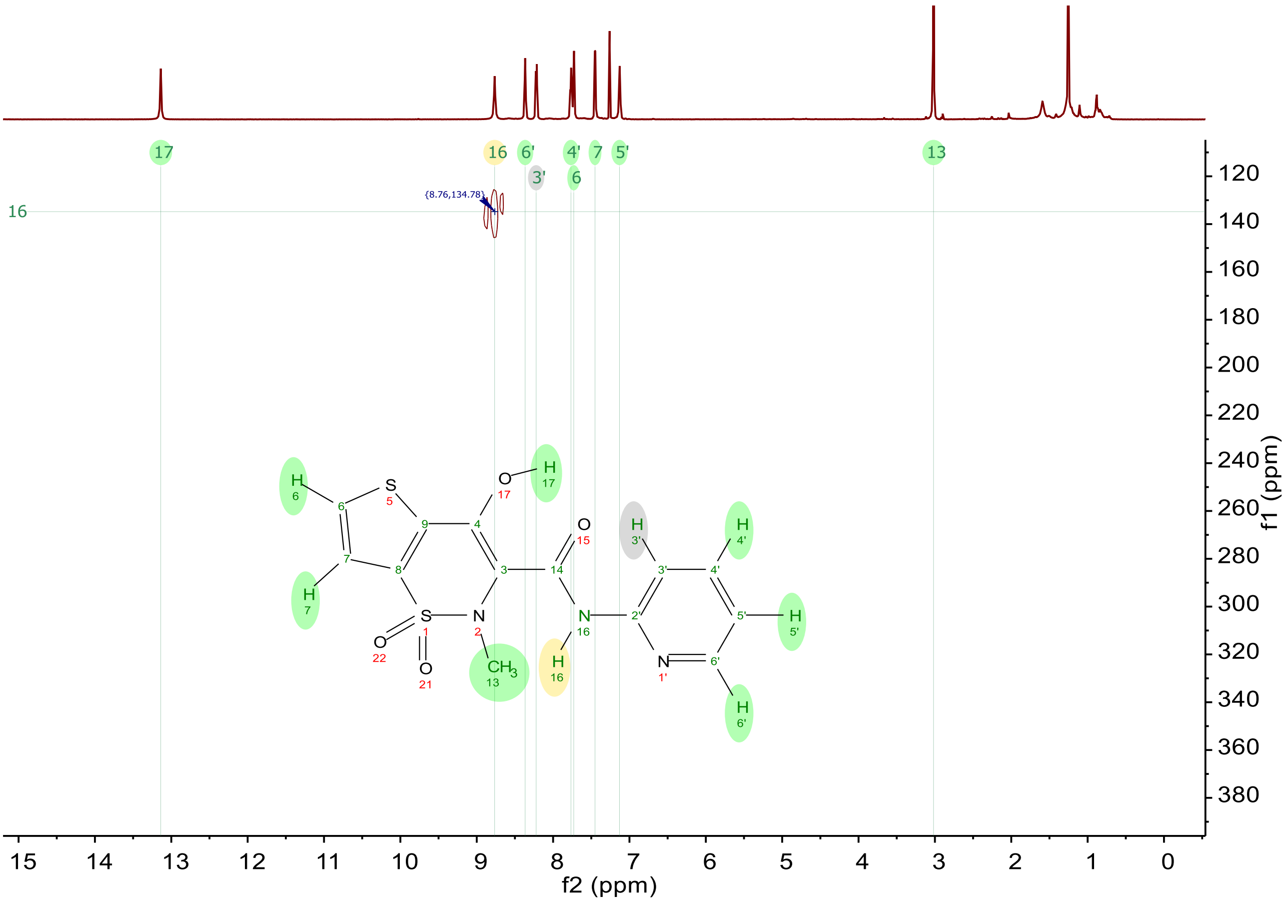

S10. Figure 700 MHz ^{1}H NMR spectrum of TXM in $CDCl_3$ at -55 °C. ZWC form of TXM is predominant at low temperature. Assignments of all protons are shown on the spectrum. Small, not assigned peaks stand for the BKE form.

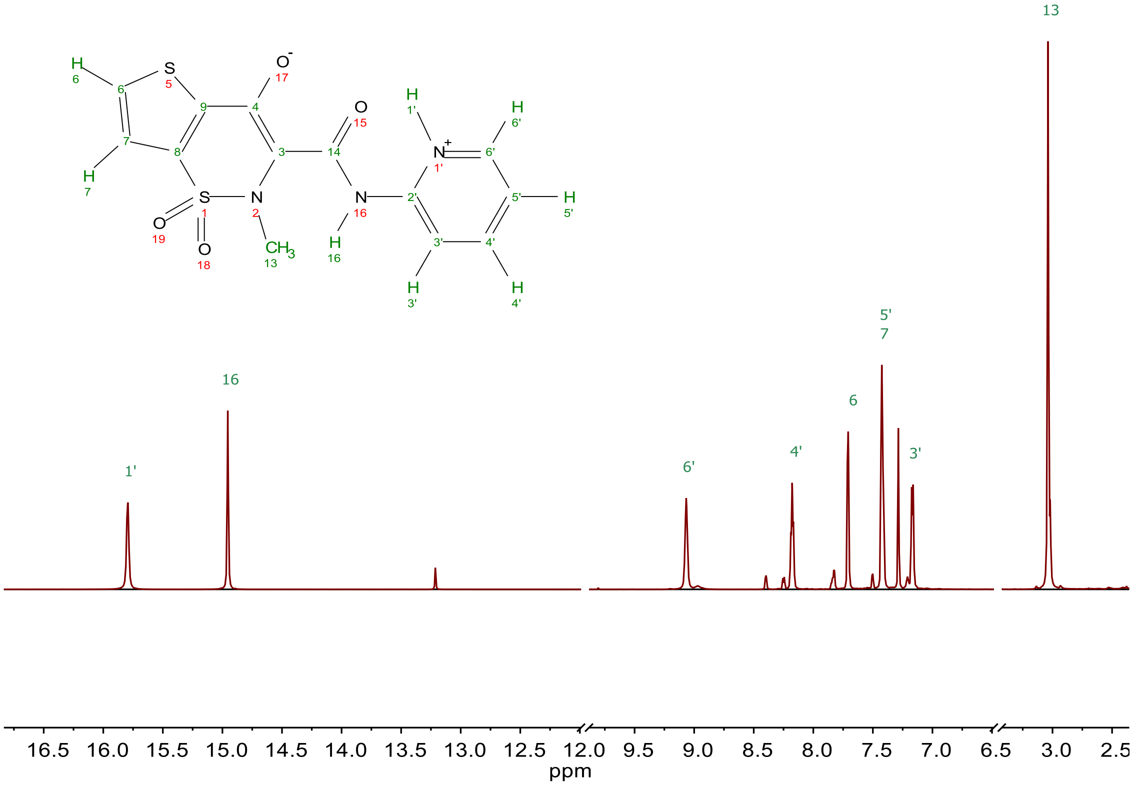

S11. Figure 176.1 MHz ^{13}C{1H} NMR spectrum of TXM in CDCl$_3$ at 25 °C. ZWC form of TXM is predominant at low temperature. Assignments of all carbons are shown on the spectrum. To suppress all ^{13}C-^{1}H scalar couplings a broadband decoupling on proton channel was applied during acquisition.

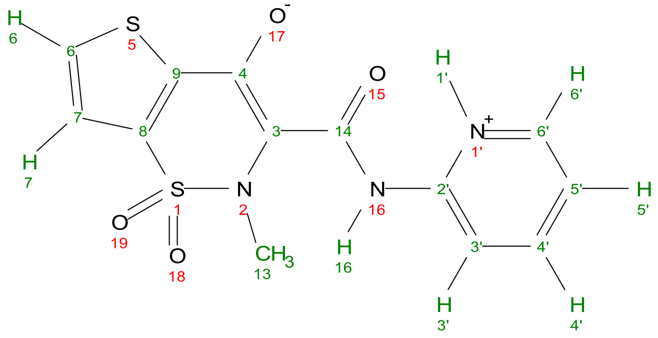

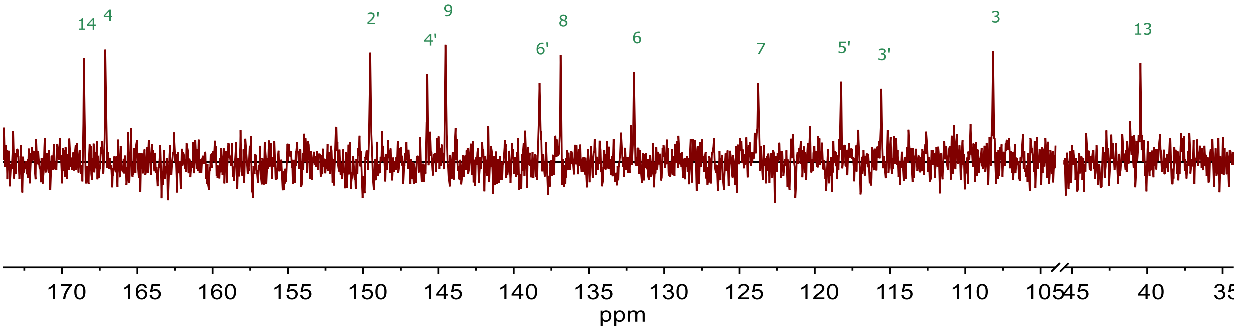

S12. Figure ^{1}H-^{13}C HSQC NMR spectrum of TXM in $CDCl_3$ at 25 °C. ZWC form of TXM is predominant at hlow temperature. Cross-peaks in HSQC spectrum indicate correlation between directly bonded protons and carbons (C-H bonds).

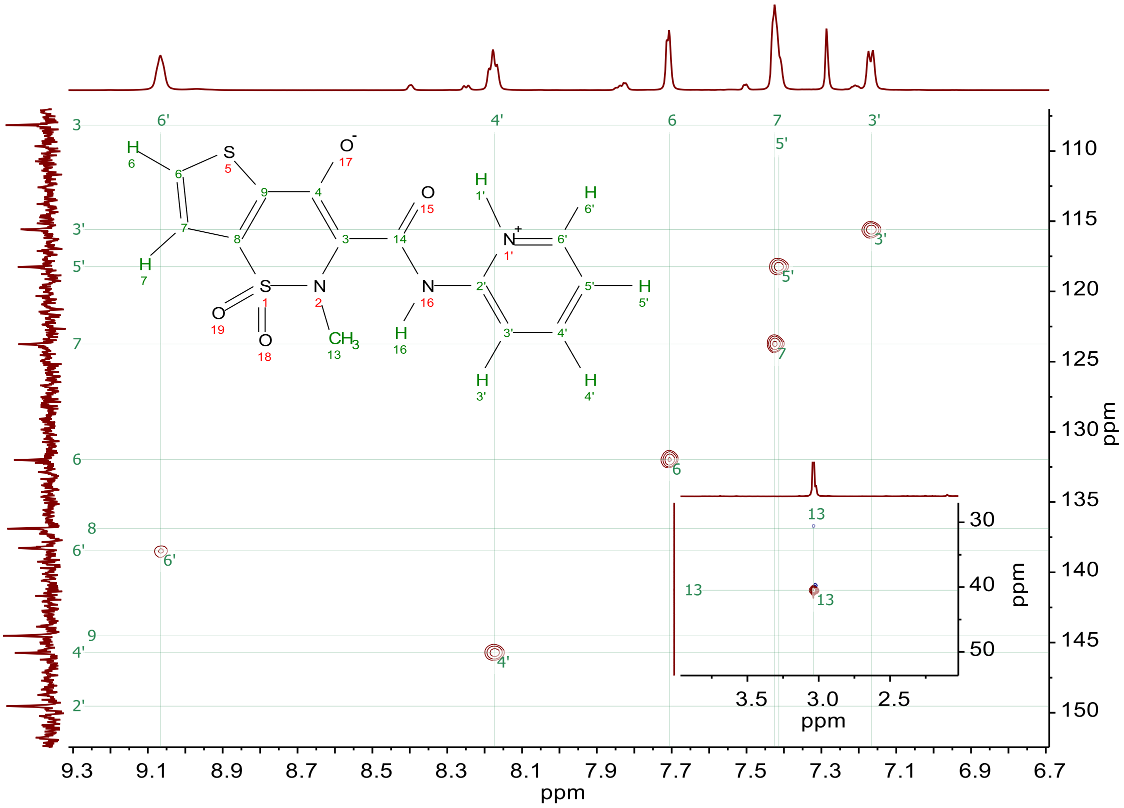

S13. Figure ^1H-^{13}C HMBC NMR spectrum of TXM in $CDCl_3$ at 25 °C. ZWC form of TXM is predominant at low temperature. Cross-peaks in HMBC spectrum indicate correlation between protons and carbons separated by 2-4 covalent bonds, while direct correlation of single-bonded protons and carbons are suppressed. HMBC allows to assign quaternary carbons and carbonyl fragments.

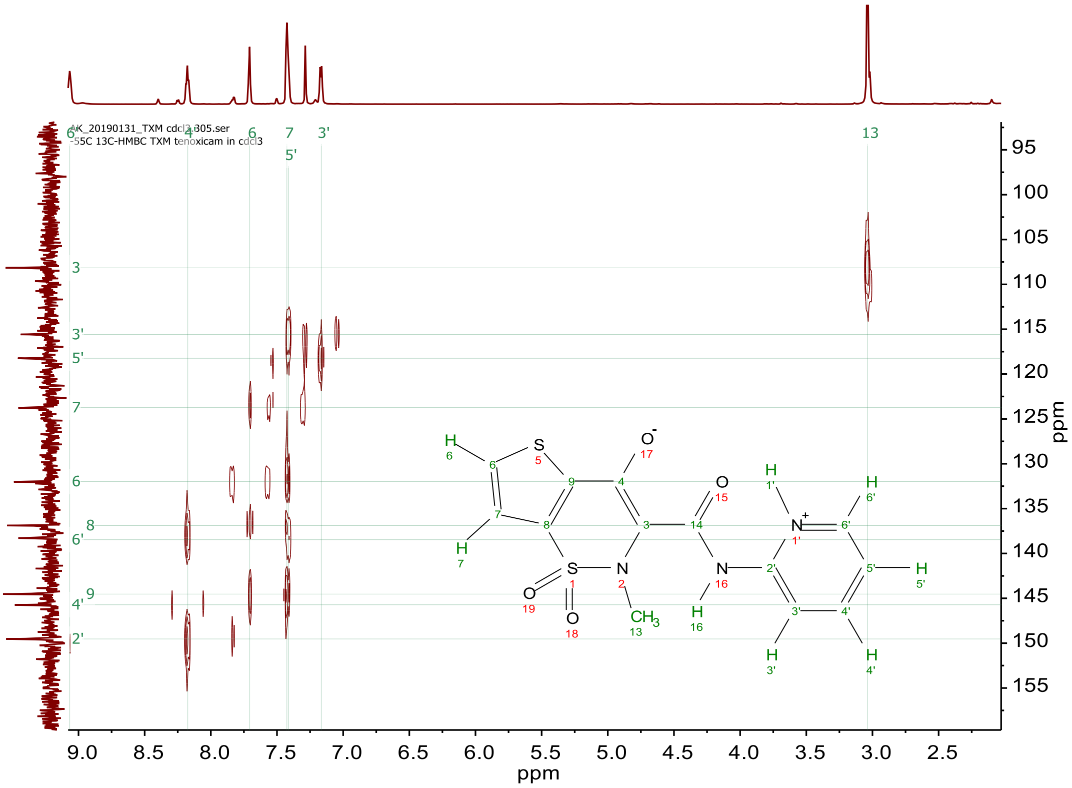

S14. Figure 700 MHz ^{1}H NMR spectrum of TXM in $CDCl_3$ at -25 °C. Both forms (ZWC and BKE) of TXM are present. Assignments of all protons are shown on the spectrum. Here “z” after nuclei number indicates ZWC, while “b” indicates BKE form.

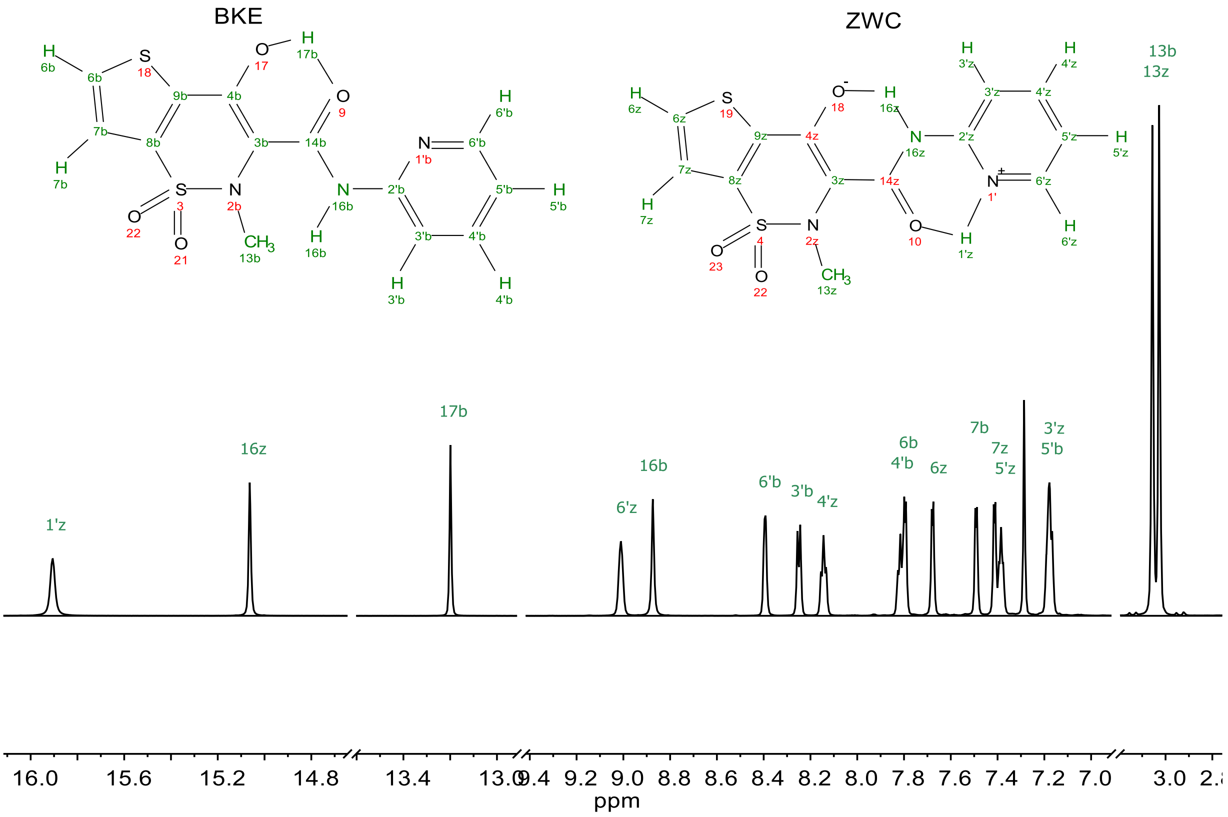

S15. Figure ^{1}H-^{13}C HSQC NMR spectrum of TXM in $CDCl_3$ at -25 °C. Both forms (ZWC and BKE) of TXM are present. Cross-peaks in HSQC spectrum indicate correlation between directly bonded protons and carbons (C-H bonds). Here “z” after nuclei number indicates ZWC, while “b” indicates BKE form.

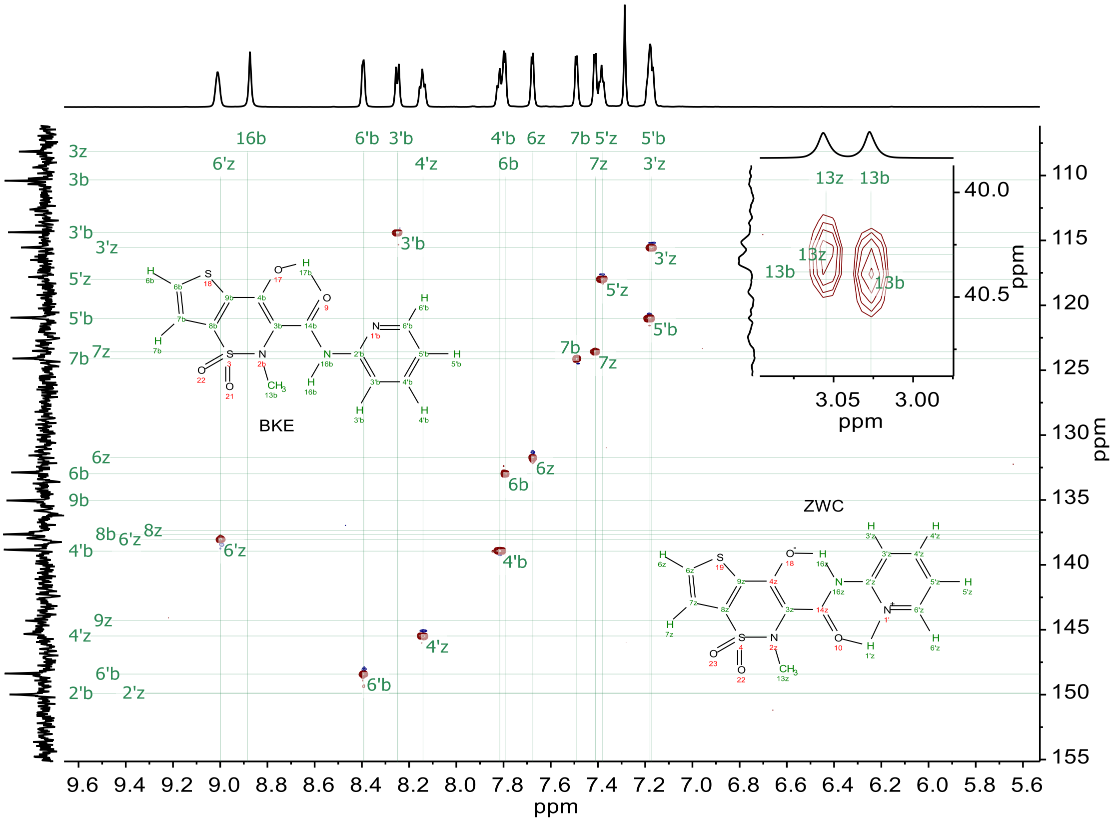

S16. Figure 700 MHz ^{1}H NMR NOESY (EXSY) spectrum of TXM in $CDCl_3$ at -25 °C. Cross-peaks in EXSY spectrum shows exchanging nuclei on a time scale of a mixing time (0.5s). Here “z” after nuclei number indicates ZWC, while “b” indicates BKE form. Labile protons 17b, 16b, 1'z are also in exchange with residual water (not shown here).

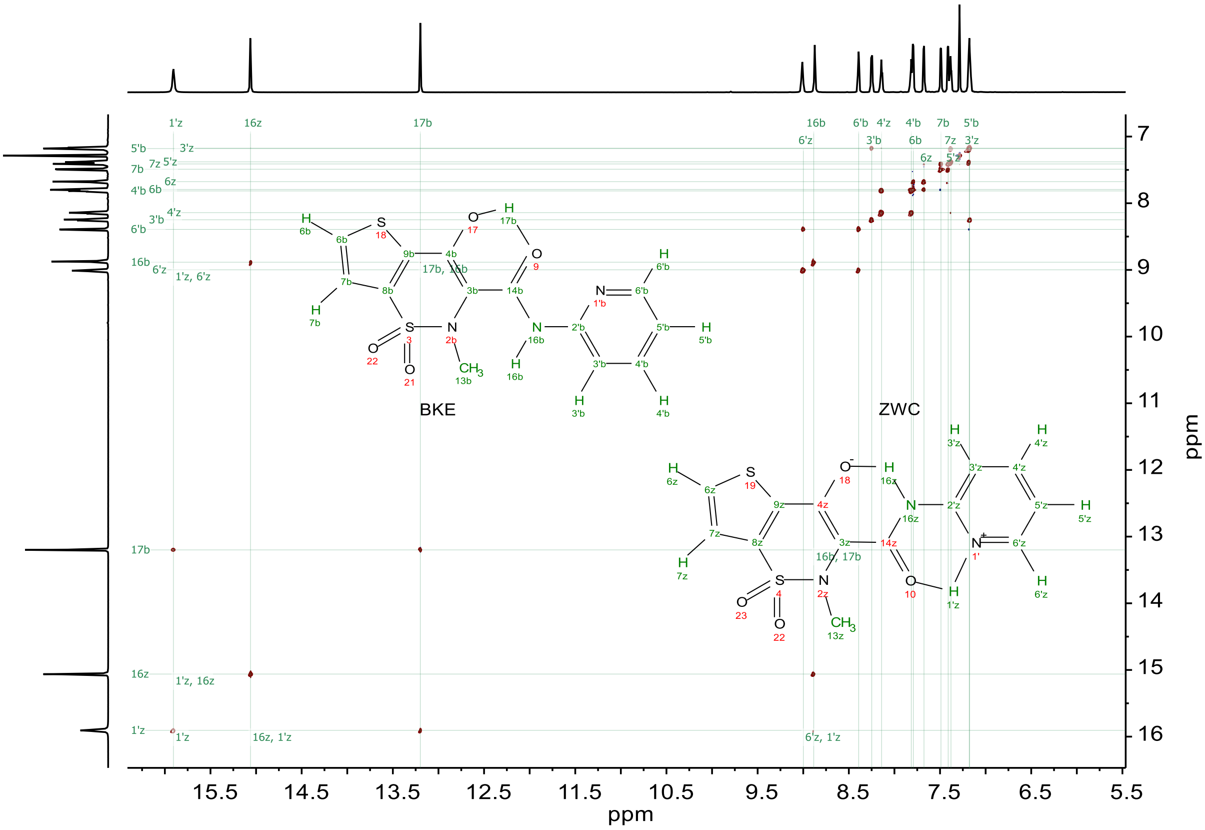

S17. Figure ^{1}H-^{15}N HSQC NMR spectrum of TXM in $CDCl_3$ at -25 °C. Both forms (ZWC and BKE) of TXM are present. Cross-peaks in ^{1}H-^{15}N HSQC spectrum indicate correlation between directly bonded protons and nitrogens (N-H bonds). In BKE form we see only one cross-peaks assigned while in ZWC form we see two cross-peaks, indeed, confirming that H17 proton moved to position H1'.

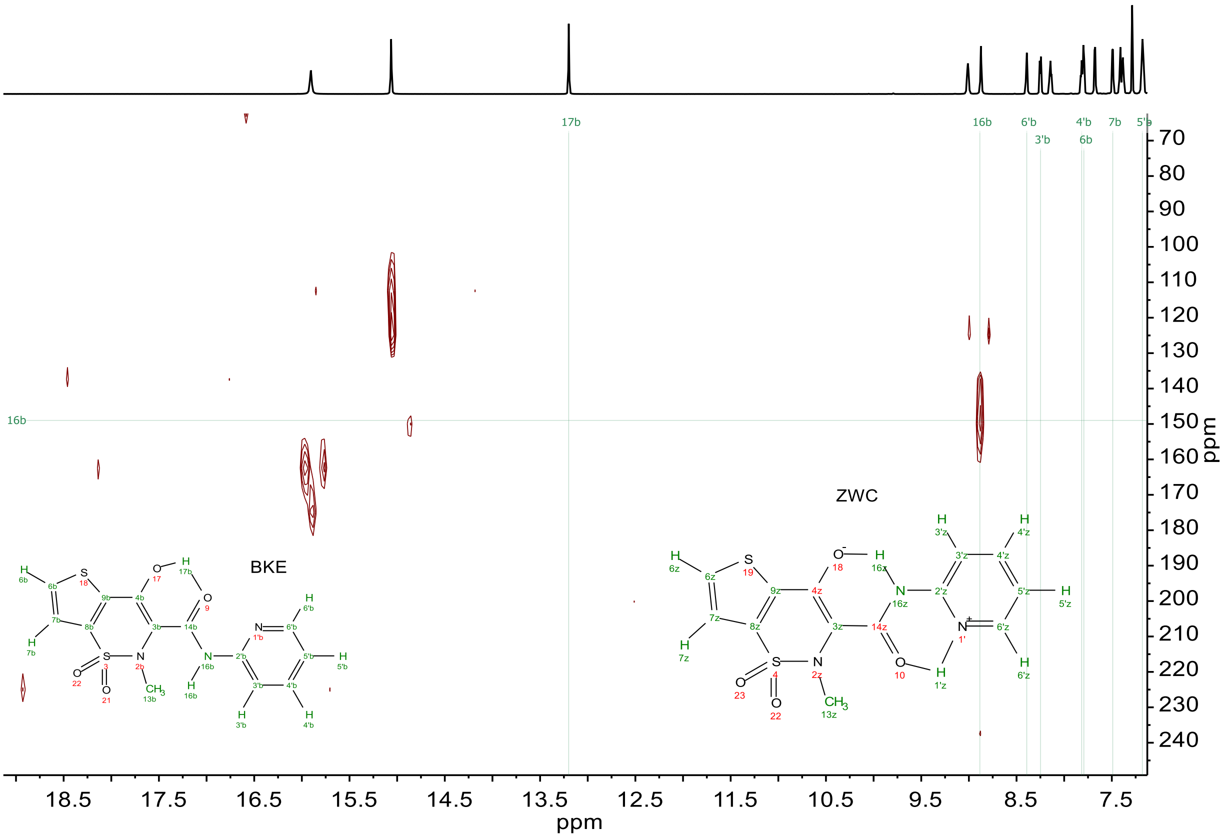

S18. Figure 700 MHz 1H NMR spectra of TXM in deuterated acetone, measured at various temperatures from -85 °C to 25 °C. Similar to spectra in chloroform (see main text) by lowering temperature two new peaks in high chemical shift region (15-16 ppm). This is an indication of hydrogen bond formation in the molecule, so ZWC form. At high temperature BKE form is dominant. At temperature -35 °C we observe broad peaks, this and indication that two forms exchange between each other.

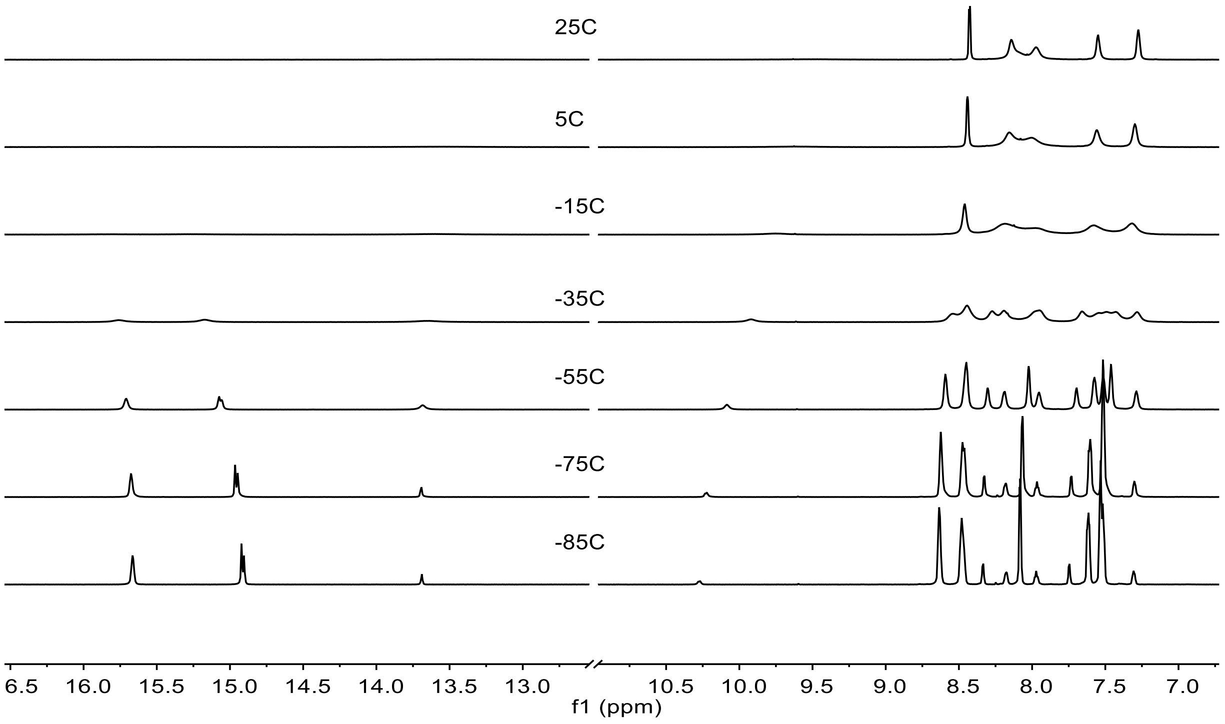

S19. Figure 700 MHz 1H NMR spectra of TXM in deuterated acetonitrile (CD_3CN), measured at various temperatures from -25 °C to 25 °C. Similar to spectra in chloroform (see main text) and in acetone by lowering temperature two new peaks in high chemical shift region (15-15.5 ppm). This is an indication of hydrogen bond formation in the molecule, so ZWC form. At high temperature BKE form is dominant. At temperature -15 °C we observe broad peaks, this and indication that two forms exchange between each other.

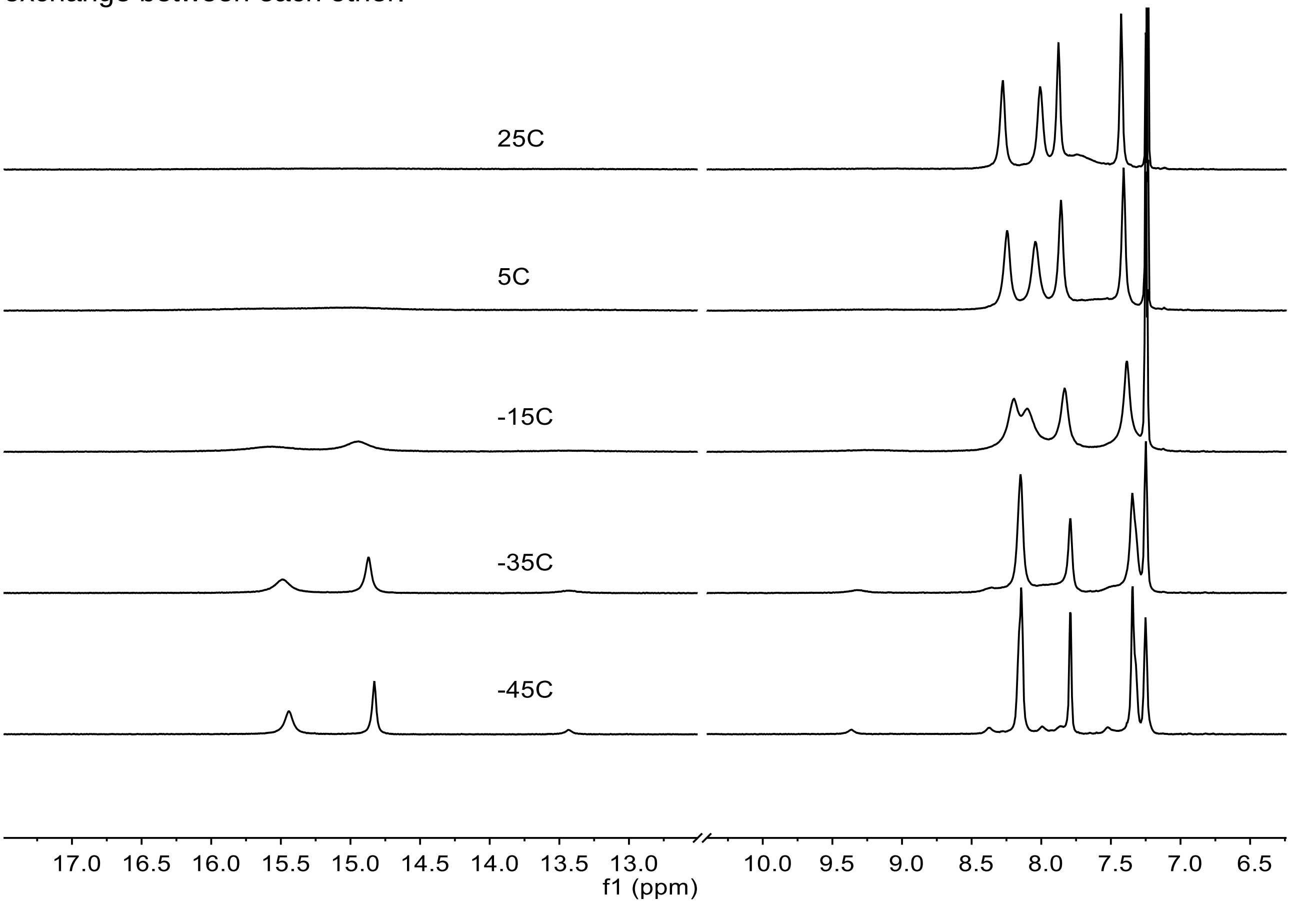

S20. Table of Crystallographic information about TXM solvates with chloroform (TXM-$CHCl_3$-I, TXM-$CHCl_3$-II, TXM-$CHCl_3$-III), acetone (TXM-ACE), N,N-dimetilformamide (TXM-DMFA) and acetonitrile (TXM-ACY); which were synthetized and solved.

	TXM-$CHCl_3$-I	**TXM-$CHCl_3$-II**	**TXM-$CHCl_3$-III**
CCDC number	1890995	1904023	1904022
Crystal data			
Chemical formula	$C_{13}H_{11}N_3O_4S_2\cdot CHCl_3$	$C_{13}H_{11}N_3O_4S_2\cdot 2(CHCl_3)$	$C_{13}H_{11}N_3O_4S_2\cdot CHCl_3$
M_r	456.74	576.10	456.74
Crystal system, space group	Monoclinic, $P2_1/c$	Orthorhombic, $P2_12_12_1$	Monoclinic, $P2_1/c$
Temperature (K)	293(2)	100(2)	100(2)
a, b, c (Å)	10.6019 (12), 12.781 (1), 28.841 (2)	9.5960 (19), 16.740 (3), 28.301 (6)	13.579 (3), 10.135 (2), 14.880 (3)
α, β, γ (°)	90, 92.076 (10), 90	90, 90, 90	90, 116.58 (3), 90
V (Å^3)	3905.5 (6)	4546.2 (16)	1831.3 (8)
Z	8	8	4
Radiation type	Mo $K\alpha$	Synchrotron, λ = 0.7937 Å	Synchrotron, λ = 0.7937 Å
μ (mm^{-1})	0.71	1.33	1.04
Crystal size (mm)	0.3 × 0.25 × 0.13	0.1 × 0.03 × 0.03	0.1 × 0.1 × 0.08
Data collection			
Diffractometer	Xcalibur, Ruby, Gemini ultra (Rigaku Oxford Diffraction, 2018)	“Belok” beamline NRC “Kurchatov Institute”	“Belok” beamline NRC “Kurchatov Institute”
Absorption correction	Multi-scan *CrysAlis PRO*	Empirical XDS (Kabsch, 2010)	Empirical XDS (Kabsch, 2010)
T_{min}, T_{max}	0.643, 1.000	0.759, 1	0.911, 1
No. of measured, independent and observed [$I > 2\sigma(I)$] reflections	54415, 6880, 2586	38347, 10006, 7832	17905, 4021, 3593
R_{int}	0.247	0.064	0.037
$(\sin \theta/\lambda)_{max}$ (Å^{-1})	0.595	0.649	0.649
Refinement			
$R[F^2 > 2\sigma(F^2)]$, $wR(F^2)$, S	0.116, 0.396, 1.03	0.064, 0.178, 1.03	0.042, 0.112, 1.06
No. of reflections	6880	10006	4021
No. of parameters	496	552	236
H-atom treatment	H-atom parameters constrained	H-atom parameters constrained	H-atom parameters constrained
$\Delta\rangle_{max}$, $\Delta\rangle_{min}$ (e Å^{-3})	0.76, -0.59	1.22, -0.89	0.34, -0.56
No. of restraints	6	0	0
	TXM-ACE	**TXM-DMFA**	**TXM-ACY**
CCDC number	1538111	1538134	1904101
Crystal data			
Chemical formula	$C_{13}H_{11}N_3O_4S_2\cdot C_3H_6O$	$C_{13}H_{11}N_3O_4S_2\cdot C_3H_7NO$	$C_{13}H_{11}N_3O_4S_2\cdot C_2H_3N$
M_r	395.44	410.46	378.42
Crystal system, space	Triclinic, $P\bar{1}$	Triclinic, $P\bar{1}$	Monoclinic, $P2_1/n$

group			
Temperature (K)	293(2)	293(2)	293(2)
a, *b*, *c* (Å)	8.9341 (4), 8.9659 (5), 11.9315 (6)	9.1060 (4), 9.4381 (4), 11.6586 (6)	9.1718 (3), 8.9965 (3), 21.1092 (8)
α, β, γ (°)	75.325 (4), 81.348 (4), 89.620 (4)	74.530 (4), 77.500 (4), 85.545 (3)	98.591 (4)
V (Å^3)	913.55 (8)	942.56 (8)	1722.26 (11)
Z	2	2	4
Radiation type	Mo $K\alpha$	Mo $K\alpha$	Mo $K\alpha$
μ (mm^{-1})	0.32	0.32	0.34
Crystal size (mm)	0.5 × 0.45 × 0.2	0.45 × 0.24 × 0.14	0.13 × 0.07 × 0.01
Data collection			
Diffractometer	Xcalibur, Ruby, Gemini ultra	Xcalibur, Ruby, Gemini ultra	Xcalibur, Ruby, Gemini ultra
Absorption correction	Multi-scan *CrysAlis PRO*	Multi-scan *CrysAlis PRO*	Multi-scan *CrysAlis PRO*
T_{min}, T_{max}	0.907, 1.000	0.827, 1.000	0.823, 1.000
No. of measured, independent and observed [$I > 2\sigma(I)$] reflections	15092, 4269, 3370	11967, 3857, 2958	26375, 3527, 2809
R_{int}	0.028	0.034	0.060
(sin $\theta/\lambda)_{max}$ (Å^{-1})	0.658	0.625	0.625
Refinement			
$R[F^2 > 2\sigma(F^2)]$, $wR(F^2)$, S	0.038, 0.108, 1.05	0.043, 0.123, 1.04	0.043, 0.101, 1.06
No. of reflections	4269	3857	3527
No. of parameters	289	257	228
H-atom treatment	H atoms treated by a mixture of independent and constrained refinement	H-atom parameters constrained	H-atom parameters constrained
$\Delta\rangle_{max}$, $\Delta\rangle_{min}$ (e Å^{-3})	0.28, -0.34	0.25, -0.30	0.043, 0.101, 1.06

S21. Hydrogen-bond geometry for described structures. Numeration as reported within crystal structures.*

TXM-CHCl$_3$-I				
D—H···*A*	*D*—H (Å)	H···*A* (Å)	*D*···*A* (Å)	*D*—H···*A* (°)
N1A—H1A···O1A	0.86	2.03	2.655 (10)	129.3
N1A—H1A···O1B	0.86	2.20	2.905 (11)	138.7
N1B—H1B···O1A	0.86	2.19	2.872 (11)	136.3
N1B—H1B···O1B	0.86	2.00	2.645 (10)	130.9
N2A—H2A···O2A	0.86	1.87	2.608 (10)	142.3
N2B—H2B···O2B	0.86	1.88	2.606 (11)	141.4
TXM-CHCl$_3$-II				
N2B—H2B···O2B	0.88	1.84	2.584 (9)	140.6
N2A—H2A···O2A	0.88	1.88	2.591 (9)	136.6
N1B—H1B···O1A^{i}	0.88	2.15	2.830 (10)	133.5
N1B—H1B···O1B	0.88	1.96	2.634 (8)	132.5
N1A—H1A···O1A	0.88	1.98	2.645 (8)	131.2
N1A—H1A···O1B^{ii}	0.88	2.12	2.797 (10)	133.5
C14B—H14B···O2B	1.00	2.07	2.963 (11)	146.8
C14A—H14A···O2A^{iii}	1.00	2.12	2.962 (12)	140.7
TXM-CHCl$_3$-III				
N2—H2···O2	0.88	1.85	2.595 (3)	141.4
N1—H1···O1^{iv}	0.88	2.21	2.893 (2)	134.5
N1—H1···O1	0.88	1.96	2.634 (2)	132.1
TXM-ACE				
N2—H2···O2	0.87 (2)	1.86 (2)	2.6098 (19)	143.0 (18)
N1—H1···O1	0.86 (2)	1.97 (2)	2.6155 (18)	130.9 (17)
N1—H1···O1^{v}	0.86 (2)	2.18 (2)	2.8767 (18)	138.2 (17)
TXM-DMFA				
N2—H2···O2	0.86	1.88	2.602 (2)	141.2
N1—H1···O1^{vi}	0.86	2.17	2.871 (2)	137.9
N1—H1···O1	0.86	1.97	2.620 (2)	131.8
TXM-ACY				
N1—H1···O1	0.86	2.00	2.641 (2)	131.1
N1—H1···O1^{vii}	0.86	2.20	2.898 (2)	138.2
N2—H2···O2	0.86	1.90	2.624 (2)	141.3

Symmetry code(s): (i) *x*-1, *y*, *z*; (ii) *x*+1, *y*, *z*; (iii) -*x*+2, *y*-1/2, -*z*+3/2; (iv) -*x*+1, -*y*+1, -*z*+2; (v) -*x*+2, -*y*+2, -*z*+1; (vi) -*x*, -*y*+1, -*z*+1; (vii) -*x*+1, -*y*+1, -*z*+1.

*Look file '*cif*' with CSD Refcode: 1890995, 1904023, 1904022, 1538111, 1538134, 1904101.

S22. Sulphur-bond geometry for described structures.

D—S···*A*	*D*—S (Å)	S···*A* (Å)	*D*···*A* (Å)
TXM-ZWC	1.27	3.03	2.81
TXM-BKE	1.33	3.06	2.82
TXM-BKE-0	1.33	3.06	2.82

S23. Comparison of experimental powder pattern of TXM chloroform solvate publicized in Patel *et. al.*[3] (1) and calculated powder pattern from solved in this work TXM-$CHCl_3$-I structure. This comparison shows that it is similar phases. Blue stars indicate picks from impurity phase in (1) sample. Experimental pattern (1) slightly shifted to the left relative to the calculated diffraction pattern (2).

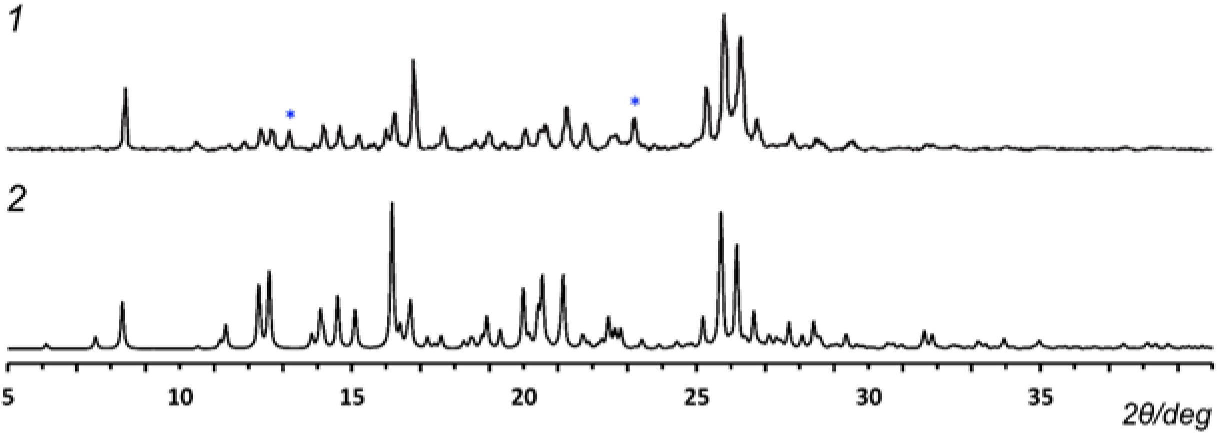

S24. Comparison of theoretical powder diffraction pattern calculated from TXM-$CHCl_3$-I structure (1) with experimental powder pattern from the phase which we call TXM-$CHCl_3$-II (2). Powder pattern (3) was recorded from the sample of TXM-$CHCl_3$-II which was warmed up at a temperature of 160 °C degrees for 1.5 hours. Powder pattern (4) belongs to the polymorph modification 1 of TXM and was taken from Patel *et al.*[3]. This picture shows that TXM-$CHCl_3$-I and TXM-$CHCl_3$-II are different phases and TXM-$CHCl_3$-II passes into the polymorph modification 1 of TXM as a result of desolvation.

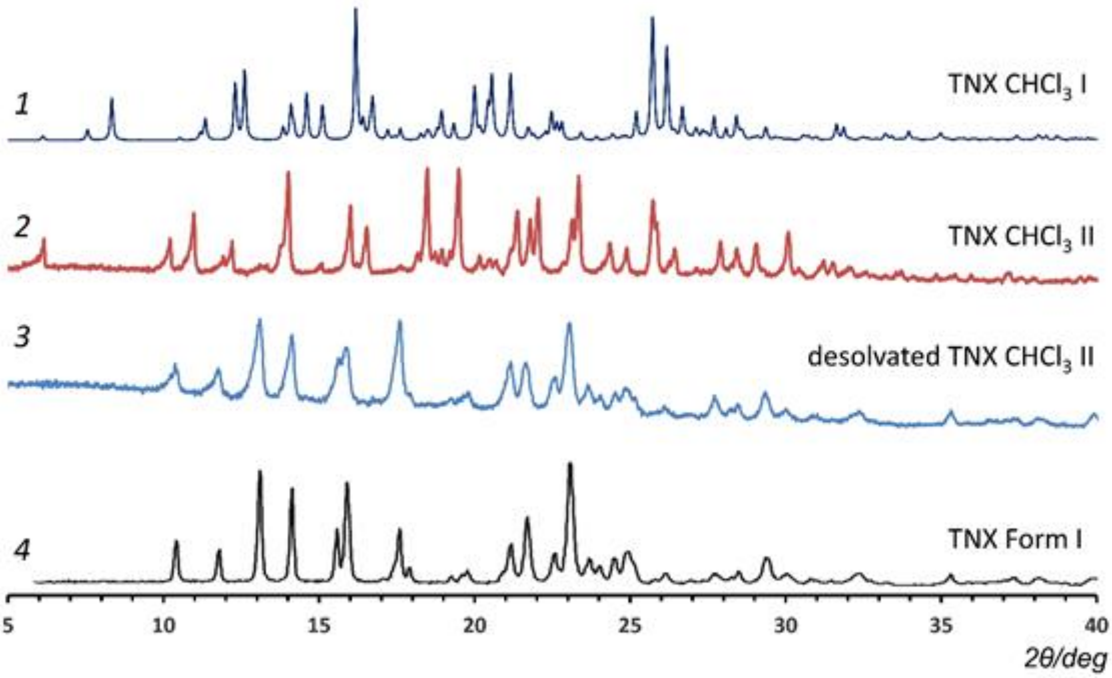

S25. Table of root-mean square deviation (RMSD) of backbone atomic position (without hydrogen atoms) in Angstrom (Å) for the tenoxicam zwitterionic form (TXM-ZWC) within solvents respect its pure form. Highlighted in green are the crystal structures solved in this article.

COFORMER/SOLVENT	RMSD (Å)
-	0
chloroform (form I)	0.091
acetonitrile	0.121
acetone	0.126
salicylic acid	0.130
N,N-dimetilformamide	0.149
benzoic acid	0.154
nitromethane	0.155
chloroform (form III)	0.171
propinoic acid	0.174
catechol	0.194
resorcinol	0.201
acetic acid	0.227
pyrogallol	0.234
chloroform (form II)	0.237
formic acid	0.245

S26. Table of Free energy (G) calculated at 298.15 K for the three full-optimized in vacuo TXM keto-enolic forms: zwitterionic (ZWC), β-keto-enolic (BKE), β-diketone.

TXM keto-enolic form	G / (kcal/mol)
ZWC	-1106709.663952
BKE	-1106711.861490
BDK	-1106699.375304

S27. Table of interaction energy calculated with perturbation theory[4] between the lone pair of H-acceptor and N—H σ* orbitals for ZWC and O—H σ* orbitals for BKE.

TXM keto-enolic form	E (kcal/mol)
ZWC	30.73
BKE	0
BKE0*	19.63

*BKE form with planar dihedral angle 1’—2’—16—14

S28. IR spectra obtained for the TXM solvate with chloroform second form (TXM-$CHCl_3$-II) without any sample preparation from 600 to 4000 cm^{-1} with the resolution of 2 cm^{-1}.

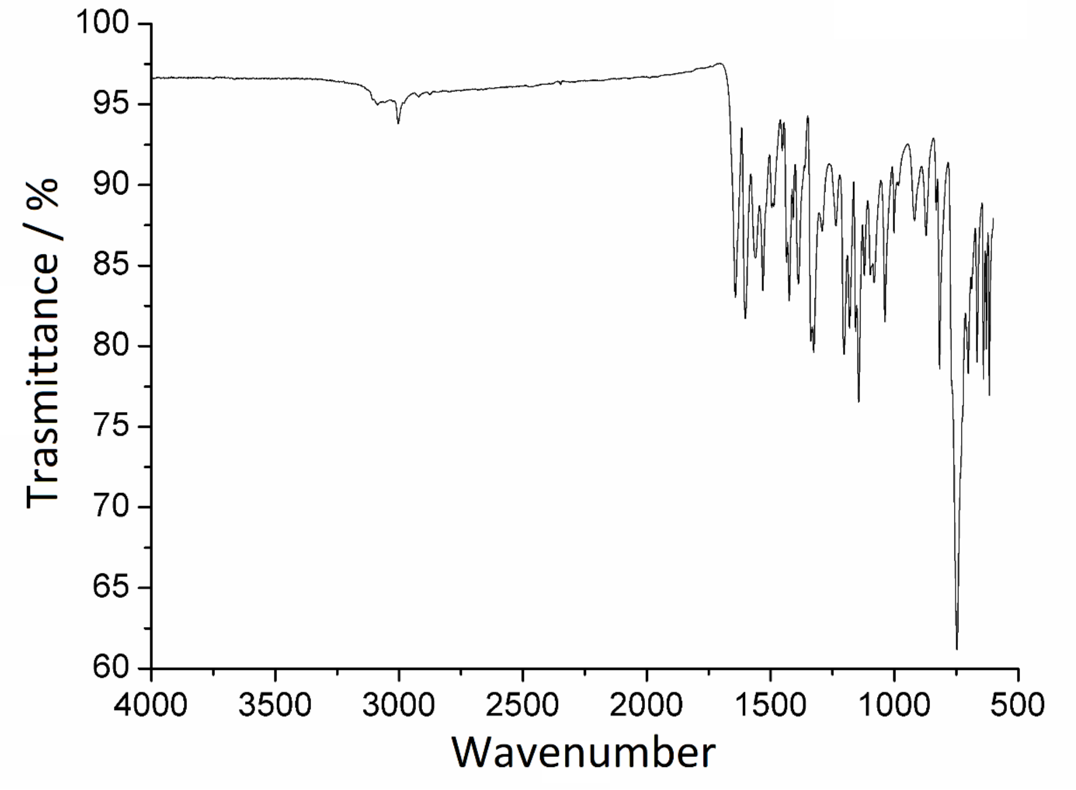

References

1. Y. Marcus, The Properties of Solvents, Jons Wiley and Sons, 1999.
2. P.S. Sherin, J. Grilj, Yu.P. Tsentalovich, E. Vauthey. *J. Phys. Chem. B.* 2009, **113**, 4953-4962.
3. J. R. Patel, R. A. Carlton, T. E. Needham, C. O. Chichester, F. G. Vogt, *Int. J. Pharm.*, 2012, 436, 685–706.
4. P. Atkins, R. Friedmann, Molecular Quantum Mechanics, Eds. Oxford University Press, 2005.